Effective Coulomb potential in SU(3) lattice Yang-Mills theory

A. Voigt,* E.-M. Ilgenfritz, and M. Müller-Preussker
Humboldt-Universität zu Berlin, Institut für Physik, D-12489 Berlin, Germany

A. Sternbeck
CSSM, School of Chemistry & Physics, The University of Adelaide, SA 5005, Australia
(Received 7 April 2008; published 3 July 2008)

We study the infrared behavior of the effective Coulomb potential in lattice SU(3) Yang-Mills theory in the Coulomb gauge. We use lattices up to a size of 48^4 and three values of the inverse coupling, $\beta = 5.8$, 6.0, and 6.2. While finite-volume effects are hardly visible in the effective Coulomb potential, scaling violations and a strong dependence on the choice of Gribov copy are observed. We obtain bounds for the Coulomb string tension that are in agreement with Zwanziger's inequality relating the Coulomb string tension to the Wilson string tension.

DOI: 10.1103/PhysRevD.78.014501 PACS numbers: 11.15.Ha, 12.38.Aw, 12.38.Gc

I. INTRODUCTION

Confinement is one of the peculiar features of quantum chromodynamics, the theory of strong interactions. Thanks to 25 years of intensive research in the field of lattice gauge theory, a few mechanisms for confinement have been identified. These mechanisms are associated either with monopoles or vortices and seem to be closely related to each other [1]. In this context, confinement was and is stated mostly by a nonvanishing string tension σ_{Wilson} which expresses the minimal energy of the gluon field between a pair of static quarks. The string tension is defined by Wilson loops and can be extracted in the limit of large Euclidean time from the Wilson-loop's area-law decay. This definition, however, is not completely satisfying, because not only quarks but also gluons are confined, and there is no area law in the more realistic case of light dynamical quarks present in the vacuum.

There are two other, though less popular, approaches that might help to shed additional light on the phenomenon of confinement. One is given by the Hamiltonian approach which promises to present an understanding not only of bound states but also of the vacuum structure in terms of wave functionals. The other is a more field-theoretically inspired approach that focuses on the QCD Green's functions and their infrared behavior. The QCD Green's functions may serve as input to a hadron phenomenology based on the Bethe-Salpeter and Faddeev equations. There, the ultimate goal is to attain a coherent description of hadronic states and processes based on the dynamics of confined gluons, ghosts, and quarks (see, e.g., Ref. [2]).

Both the Hamiltonian approach and investigations of QCD Green's functions require to fix a gauge. This introduces the well-known Gribov ambiguity present in the Coulomb as well as in covariant gauges. One should keep in mind that the confinement mechanisms associated with monopoles and vortices, that received credit by reproducing the Wilson string tension, also mostly require a gauge condition. In the Coulomb gauge, the Gribov ambiguity represents a severe source of uncertainty and its effect on the results must be faithfully checked. On the other hand, the Coulomb gauge yields a particularly interesting confinement picture called the Gribov-Zwanziger scenario [3,4]. This scenario might provide an understanding of confinement even in the presence of dynamical quarks when the Wilson-loop criterion fails.

A central element of the Gribov-Zwanziger confinement scenario in Coulomb gauge is the instantaneous color-Coulomb potential involving the Faddeev-Popov operator M (in Coulomb gauge) and the infrared spectral properties of the latter [5,6]. The expression

$$V_{\text{Coul}}(x-y)\delta^{ab} = \langle g^2[M^{-1}(-\triangle)M^{-1}]^{ab}(x,y)\rangle \qquad (1)$$

is defined through the vacuum expectation value of the potential part of the Hamilton operator

$$H = \frac{1}{2}\int d^3x(\vec{\Pi}^2_{\text{tr}}(\vec{x}) + \vec{B}^2(\vec{x})) + H_{\text{Coul}} \qquad (2)$$

resulting from the elimination of longitudinal degrees of freedom. Here the potential term H_{Coul} is expressed in terms of the color-charge density (including external sources and the charge density of the gluon field itself) by means of the color-Coulomb potential,

$$H_{\text{Coul}} = \frac{1}{2}\int d^3x d^3y \rho^a(\vec{x}) V_{\text{Coul}}(x-y)\delta^{ab}\rho^b(\vec{y}). \qquad (3)$$

As Zwanziger has shown [4], the Coulomb potential does not equal the Wilson potential V_{Wilson} used to extract the string tension σ_{Wilson} as an order parameter for confinement. Instead, for large spatial distances r the Coulomb potential represents an upper bound for the rise of the Wilson potential,

*Present address: Max-Planck-Institut für Meteorologie, D-20146 Hamburg, Germany.

$$V_{\text{Wilson}}(r) \leq -\tfrac{4}{3} V_{\text{Coul}}(r). \tag{4}$$

In other words, there is no confinement without Coulomb confinement since the Coulomb string tension is an upper bound for the Wilson string tension [7],

$$\sigma_{\text{Wilson}} \leq \tfrac{4}{3} \sigma_{\text{Coul}}. \tag{5}$$

Zwanziger has continuously developed the confinement scenario originally proposed by Gribov [3]. He has put forward the Coulomb potential as a new order parameter for confinement [4,7,8]. In fact, the Coulomb potential is expected to linearly rise at large r even in the presence of dynamical quarks when the Wilson-loop criterion fails. Recent lattice studies have shown, however, that the relation (4) is only a *necessary* [9] condition for confinement, and that the Coulomb potential can be linearly rising with spatial distance even in the deconfinement phase [6,10].

Using lattice techniques, a linearly rising Coulomb potential [9–11] and a connection between the center-vortex mechanism and the Gribov-Zwanziger scenario [5,12,13] have been observed. Furthermore, Greensite *et al.* proposed [14] to use correlators of partial Polyakov loops to measure the Coulomb potential. Corresponding SU(2) as well as SU(3) studies revealed that the Coulomb string tension σ_{Coul} could well be 2–3 times larger than the Wilson string tension σ_{Wilson} [10–12,14]. This is in contrast to results of SU(2) studies where the Coulomb potential was measured by means of its very definition via Eq. (1) suggesting $\sigma_{\text{Coul}} = \sigma_{\text{Wilson}}$ [15,16]. In the present study we provide a (yet missing) thorough measurement of the Coulomb potential in SU(3) gauge theory based on its very definition in Eq. (1). We investigate the relation between σ_{Wilson} and σ_{Coul} and find, though hedged with large uncertainty, σ_{Coul} to be 1.6 times larger than σ_{Wilson}. The origin of the systematic uncertainty will be discussed.

The paper is organized as follows. In Sec. II we describe the details of our numerical simulation and define the lattice observables measured. We investigate finite-volume effects, lattice-spacing effects and the effects due to the Gribov ambiguity in Sec. III. In Sec. IV we analyze the infrared behavior of the effective Coulomb potential. A summary concludes this paper.

II. DETAILS OF THE NUMERICAL SIMULATION

A. Lattice samples and gauge-fixing algorithms

For our study we use the standard lattice formulation of SU(3) Yang-Mills theory in Coulomb gauge where we always start from nongauge-fixed SU(3) gauge configurations and apply the Coulomb gauge condition subsequently. Our sets of gauge configurations were generated with Wilson's one-plaquette action at three values of the inverse coupling, $\beta = 5.8$, 6.0, and 6.2, for a couple of lattice sizes $L_s^3 \times L_t$ where L_t and L_s denote the spatial and temporal lattice extension, respectively. We have only considered hypercubic lattices with $L_s = L_t = L = 12$, 16, 24, 32, and 48. Those ensembles were then gauge fixed to the Coulomb gauge by minimizing the gauge functional

$$F_U[g] = \frac{1}{3} \sum_x \sum_{i=1}^{3} \text{Re Tr}(1 - g_x U_{x,i} g^\dagger_{x+\hat{i}}), \tag{6}$$

that involves all spacelike links on the lattice. This was accomplished by adjusting the gauge transformations $g_x \in \text{SU(3)}$ while keeping the original gauge configuration U fixed. Because of the particular form of $F_U[g]$ no condition is imposed on timelike links. Consequently, the different time slices can be minimized independently. We considered gauge fixing within a given time slice successful as soon as the stopping criterion

$$\max_{\vec{x},t \text{ fix}} \text{Tr}[(\partial_i {}^g A_{x,i})(\partial_i {}^g A_{x,i})^\dagger] < 10^{-13} \tag{7}$$

was satisfied. Here the lattice gauge-potential is defined in the usual way as

$${}^g A_{x+\hat{i}/2,i} = \frac{1}{2iag_0} ({}^g U_{x,i} - {}^g U^\dagger_{x,i}) \Big|_{\text{traceless}}, \tag{8}$$

where ${}^g U_{x,i} \equiv g_x U_{x,i} g^\dagger_{x+\hat{i}}$, a is the lattice spacing and g_0 the bare coupling constant which is related to β through $\beta = 6/g_0^2$.

To minimize the gauge functional we used an over-relaxation (OR) algorithm preceded by an optimally tuned simulated annealing (SA) algorithm. In what follows, we call this particular combination of simulated annealing and over-relaxation steps the SA-OR algorithm. To assess the influence of Gribov copies, we also generated some gauge copies with the pure OR algorithm without preconditioning. In all cases, the over-relaxation parameter was tuned to $\omega = 1.70$ on the small and $\omega = 1.60$ on the large lattices. More details are given below.

The SA algorithm has been proven to be very useful in handling various optimization problems. For this algorithm the gauge functional $F_U[g]$ is regarded as a "spin Hamiltonian" where the gauge transformation fields g_x take the role of "spin variables" coupled through the links $U_{x,i}$ (kept fixed). Minimizing $F_U[g]$ is achieved by adiabatically lowering the auxiliary temperature T of a statistical spin glass system characterized by the Gibbs weight

$$W[g] \propto \exp(-F_U[g]/T). \tag{9}$$

The minimization process always starts with equilibrating this spin system at some initial temperature $T = T_i$ which is then slowly decreased. Formally, in the limit of (adiabatically) lowering $T \to 0$ this system approaches the ground state and hence the gauge functional reaches its absolute minimum for a given gauge configuration. For the practical purpose considered here, such an adiabatic cooling-down process is not feasible as it would require an enormous amount of computing time. Nevertheless, we find that much lower minima for $F_U[g]$ can be reached, compared to applying only over-relaxation (OR), if we

combine the SA with the OR algorithm as follows: We start from an initial temperature of $T_i = 0.45$ and linearly decrease the temperature down to $T_f = 0.01$ within 1500 "compound sweeps." Each such sweep consists of one heatbath and three microcanonical update sweeps. After this, we use the OR algorithm until the Coulomb gauge is reached, i.e. the stopping criterion (7) is satisfied.

The advantage of using the SA-OR instead of the OR algorithm alone becomes more pronounced as the lattice becomes larger. Furthermore, the number of necessary iterations in the subsequent OR algorithm is drastically reduced by a preceding SA algorithm, the more the lower the final T_f is chosen. Note that instead of adding subsequent OR steps, we could also have used SA on its own extending its use to a much lower temperature T_f to fix to Coulomb gauge. This, however, is much more CPU-time intensive and we find no benefit in doing this, because after gauge fixing the transversality condition (7) must at any case be guaranteed with high precision, which can be achieved only by the finalizing OR.

We observe that the time slices of a given configuration may behave very differently during the iterative gauge-fixing process. In fact, we find the number of necessary iterations may differ by a factor of 10 to 20 between the individual time slices of a given configuration. In the majority of cases, time slices did not show any recalcitrancy during gauge fixing, although in some cases time slices could not be fixed within a certain (predefined) number of iterations. In the latter case we simply repeated the entire gauge-fixing process for *these* time slices, using the same algorithm but starting from a different randomly chosen gauge transformation. The "well-behaved" and hence already gauge-fixed time slices were not touched again.

After all individual time slices had been minimized, the original configuration U was gauge transformed, i.e., $U_{x,\mu} \rightarrow {}^{g}U_{x,\mu}$. To simplify the notation we drop the label g in what follows and assume that a gauge configuration U satisfies the Coulomb gauge condition already. Since our observables, namely, the effective Coulomb potential and the ghost propagator, are genuine three-dimensional, instantaneous observables defined by spacelike links only, we did not have to fix the residual gauge freedom. The latter, after the Coulomb gauge has been fixed, resides in spatially constant but time-dependent gauge transformations (for a continuum view at this problem see [17]).

B. Observables of interest

The Coulomb energy is a complicated functional of the transverse gauge potential $A_i(\vec{x})$ and the total color-charge density. Nevertheless, it is instructive to characterize its gross features through the infrared and ultraviolet behavior of the expectation value of the color-diagonal part of the kernel $M^{-1}(-\triangle)M^{-1}$ in momentum space alone. On the lattice this is defined as the MC average

$$V^L_{\mathrm{Coul}}(\vec{k}) = \frac{1}{8L_s^3}\left\langle \sum_{a,\vec{x},\vec{y}} e^{i\vec{k}\cdot(\vec{x}-\vec{y})}[M^{-1}(-\triangle)M^{-1}]^{aa}_{\vec{x}\,\vec{y}} \right\rangle, \quad (10)$$

where we use a shorthand notation for the scalar product $\vec{k}\cdot\vec{x} = 2\pi\sum_{i=1}^{3} k_i x_i/L_i$ with integer-valued lattice momenta k_i and lattice coordinates x_i. M is the lattice Faddeev-Popov operator for the Coulomb gauge

$$M^{ab}_{xy} = \delta_{x_4,y_4}\sum_{i=1}^{3}\mathrm{Re\,Tr}[\{T^a, T^b\}(U_{x,i} + U_{x-\hat{i},i})\delta_{\vec{x},\vec{y}} - 2T^bT^aU_{x,i}\delta_{\vec{x}+\hat{i},\vec{y}} - 2T^aT^bU_{x-\hat{i},i}\delta_{\vec{x}-\hat{i},\vec{y}}]. \quad (11)$$

Note that the Faddeev-Popov operator is a direct sum of operators acting within individual time slices. In coordinate space these three-dimensional operators define the Coulomb energy of a given dynamical (gluonic) color-charge density plus an external one [cf. Eq. (3)]. Given the tree-level form of the Coulomb potential on a three-dimensional lattice we relate integer-valued lattice momenta $k_i \in (-L_i/2, L_i/2]$ to physical ones by

$$q_i(k_i) = \frac{2}{a}\sin\left(\frac{\pi k_i}{L_i}\right). \quad (12)$$

Physical units are assigned by using the interpolation formula for r_0/a as given in [18] setting $r_0 = 0.5$ fm. To simplify the writing we introduce q as abbreviation for $|\vec{q}|$ whenever appropriate.

In Ref. [8] an analytic calculation of the Coulomb potential is presented which reads, upon Fourier transformation,

$$V_{\mathrm{Coul}}(q) = q^2G^2(q) + V^{\mathrm{c}}(q). \quad (13)$$

Here G denotes the ghost propagator (entering the disconnected part) and V^{c} denotes the connected part of the potential. Under the assumption that the (yet unknown) connected part can be neglected, an infrared asymptotic limit for V_{Coul} has been given in [8]. It will be analyzed below at what momenta the factorization $V_{\mathrm{Coul}}(q) \simeq q^2G^2(q)$ is justified from our data concerning both the effective Coulomb potential and the ghost propagator. The latter can be estimated in momentum space as the MC average

$$G^L(\vec{k}) = \frac{1}{8L_s^3}\left\langle \sum_{a,\vec{x},\vec{y}} e^{i\vec{k}\cdot(\vec{x}-\vec{y})}[M^{-1}]^{aa}_{\vec{x}\,\vec{y}} \right\rangle \quad (14)$$

at nonzero lattice momenta k. As for the Coulomb potential we use Eq. (12) to assign physical momenta to G. To invert the Faddeev-Popov operator we adapted the techniques developed in Landau-gauge studies of the ghost propagator (see, e.g., [19]). The data for the ghost propagator used to test the factorization hypothesis will not be presented in the present publication. They have been presented at Lattice 2007 [20] and will be discussed more in depth in a forthcoming paper [21].

Note that both the evaluation of the effective Coulomb potential and of the ghost propagator involve CPU-time intensive operations. As a consequence, we have restricted our measurements to lattice momenta k that survive a cylinder cut. Our cylinder cut is the obvious adaptation of the Landau-gauge cylinder cut [22]. To minimize finite-volume effects, we also cone cut our data [22] if they refer to lattices smaller than $(2.5\ \mathrm{fm})^4$.

C. Running coupling and physical scale

The Coulomb potential is a renormalization-group invariant which can be written as [here for pure SU(3) gauge theory] [23]

$$q^2 V_{\mathrm{Coul}}(q) = \frac{12}{11} g^2_{\mathrm{Coul}}(q/\Lambda_{\mathrm{Coul}}), \tag{15}$$

where Λ_{Coul} is a special QCD scale parameter characteristic of the Coulomb gauge, that defines a running coupling constant g_{Coul}. The latter has to satisfy the renormalization-group equation

$$q \frac{\partial g_{\mathrm{Coul}}}{\partial q} = \beta_{\mathrm{Coul}}(g_{\mathrm{Coul}}), \tag{16}$$

where the beta function, β_{Coul}, has the usual weak-coupling expansion starting with the two standard scheme-independent coefficients

$$b_0 \equiv \frac{11}{16\pi^2} \quad \text{and} \quad b_1 \equiv \frac{51}{128\pi^4} \tag{17}$$

(see [23] for higher terms). For sufficiently large q, the product $11 q^2 V_{\mathrm{Coul}}(q)/12$ is expected to be described through the two-loop expression of the running coupling

$$g^2_{\mathrm{Coul}}(q) = \frac{1}{b_0 \ln(q^2/\Lambda^2_{\mathrm{Coul}})}\left[1 - \frac{b_1}{b_0^2}\frac{\ln[\ln(q^2/\Lambda^2_{\mathrm{Coul}})]}{\ln(q^2/\Lambda^2_{\mathrm{Coul}})}\right]. \tag{18}$$

Lattice data describing $q^2 V_{\mathrm{Coul}}(q)$ do not depend on the lattice spacing a in the asymptotic scaling region. At larger a, scaling violations should be expected though, and they will be discussed below for the lattice spacings used in this study.

In a previous analysis of the data [20] we used an ultraviolet fit to the one-loop expression [cf. the first term of Eq. (18)] to fix the unknown physical scale of the effective Coulomb potential (see Ref. [20] for details). For the present study, we scrutinized if the highest momenta accessible in our simulations really permit a feasible fit to the one-loop or the two-loop expression given in Eq. (18). We find that this is not the case and that the ultraviolet fit described in [20] has artificially up-scaled our data by a free factor bigger than one. In the present study, we therefore do not rely anymore on this ultraviolet fit.

Indeed, the physical scale is fixed by simply multiplying the bare lattice data for the effective Coulomb potential with $6/(\beta a^2)$:

$$V_{\mathrm{Coul}}(q) = \frac{6}{\beta} a^2 V^L_{\mathrm{Coul}}(k, \beta), \tag{19}$$

where a denotes the lattice spacing in GeV^{-1}. Again, we use the interpolation formula in [18] to set a assuming $r_0 = 0.5$ fm. For all figures in the present paper, the physical scale of the effective Coulomb potential is fixed in this way.

III. STUDYING SYSTEMATIC EFFECTS

In this section we discuss the effects of finite lattice volumes and lattice spacings as well as the influence of the Gribov ambiguity on the effective Coulomb potential.

A. Lattice artifacts

As we are primarily interested in the product $q^4 V_{\mathrm{Coul}}(q)$, we directly discuss this product instead of the effective Coulomb potential itself. Note that we investigate effects of finite lattice spacings and volumes by considering Coulomb-potential data collected for first SA-OR copies only.

Finite-volume effects are studied by varying the lattice sizes from 12^4 to 48^4 but keeping β, and hence the lattice spacing a, fixed. We find that only data obtained on the smaller lattices, 12^4 and 16^4, at $\beta = 6.0$ show visible finite-volume effects at lower momenta. For larger lattices, namely 24^4, 32^4, and 48^4, effects seem to be mild (see the magnified view in the right panel of Fig. 1). At $\beta = 5.8$ (reaching even lower momenta) only the 12^4 data clearly deviate from the other data (see Fig. 1, left panel).

Lattice-spacing effects are investigated by comparing data from lattices of equal physical volume for different values of β. Within our choice of β values and lattice sizes L^4, we can find only a few combinations of β and L where this is approximately possible. For those we can compare data at approximately equal physical momenta and disentangle by eye the effect of varying a. As demonstrated in Fig. 2 these discretization effects are small and of the order of 10% to 15% at largest. The difference between data for $\beta = 6.2$ and 6.0 is smaller (right panel) than the difference between data for $\beta = 6.0$ and 5.8 (left panel).

B. Effects due to the Gribov ambiguity

In comparison to lattice artifacts, the Gribov ambiguity turns out to have a much larger impact on the Coulomb potential data. In order to assess the influence of this ambiguity, we follow the "first-copy—best-copy" (fc-bc) strategy applied before in Landau-gauge studies of gluon and ghost propagators [19,24]. Here, we use this strategy in two different ways.

First, we estimate the number N_{cp} of gauge-fixed copies per configuration necessary to achieve "quasiconvergence" of the Coulomb potential, considered as a function

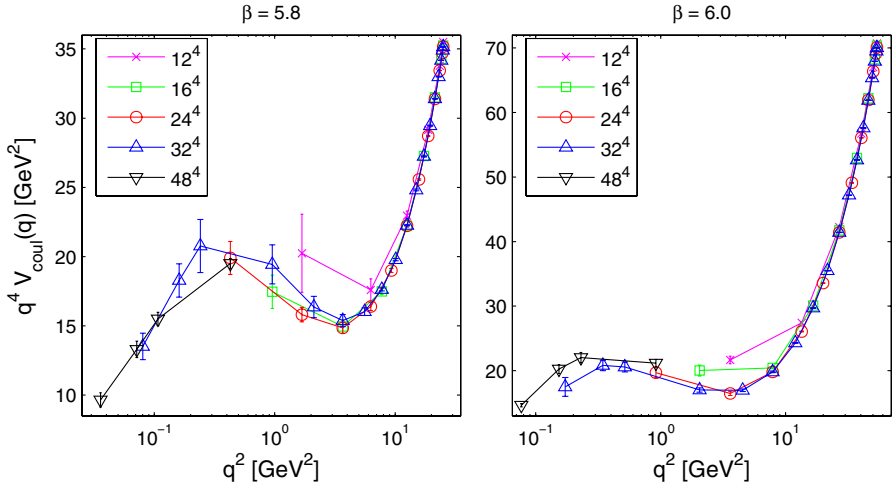

FIG. 1 (color online). The Coulomb potential multiplied by q^4 shown as a function of q^2 in physical units. We show data for different lattice sizes at $\beta = 5.8$ (left) and $\beta = 6.0$ (right) to illustrate finite-volume effects. These seem to be under control for data on lattices larger than 16^4 because those fall roughly on the same curve. For both β values we only used data from first SA-OR copies (fc).

of N_{cp}. Second, we quantify the systematic error of the Coulomb potential that is admitted if *an arbitrary* (first) gauge-fixed copy is chosen instead of *the best* copy among N_{cp} copies for each gauge configuration. A copy is considered to be the best among all N_{cp} gauge-fixed copies of a given configuration if its gauge functional is lower than those of all the other $N_{\mathrm{cp}} - 1$ copies after the gauge-fixing has been attempted N_{cp} times.

Let us first compare the convergence of the bare data describing the Coulomb potential upon increasing $N_{\mathrm{cp}} \rightarrow N_{\mathrm{cp}}^{\mathrm{max}}$ for the two gauge-fixing algorithms OR and SA-OR. As an example, in Fig. 3 we show for each lattice size data describing V_{Coul} for the lowest (on-axis) lattice momentum available, i.e. $\vec{k} = ([1, 0, 0])$ with square brackets indicating that the average over all permutations is taken. Note that in contrast to the rest of this paper we did not apply neither the cylinder nor the cone cut here. The obtained deviations from the best-copy value can be considered as an upper bound for all other momenta.

The data were obtained at $\beta = 6.0$ on lattice sizes $L^4 = 12^4$, 16^4, and 24^4. For each gauge-field configuration a number of $N_{\mathrm{cp}}^{\mathrm{max}} = 20$, 30, and 40 independent gauge-fixed copies was generated separately with the OR and the SA-OR algorithm. From the figure we see that upon increasing N_{cp} the effective Coulomb potential decreases and becomes (more or less) independent of N_{cp} for N_{cp} coming closer to $N_{\mathrm{cp}}^{\mathrm{max}}$. What N_{cp} is sufficient to achieve quasiconvergence depends, of course, on the gauge-fixing algorithm and on the lattice size. In fact, it is clearly visible in Fig. 3 that the number of gauge copies necessary to achieve convergence is substantially lower for the SA-OR algo-

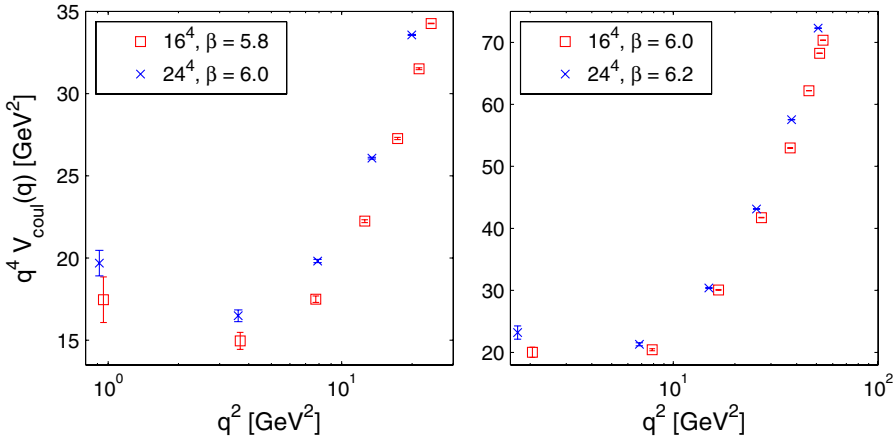

FIG. 2 (color online). The Coulomb potential multiplied by q^4 shown versus q^2 measured on comparable physical volumes. Data for $\beta = 5.8$ and 6.0 are shown on the left, and for $\beta = 6.0$ and 6.2 on the right-hand side. Only data from first SA-OR copies is shown.

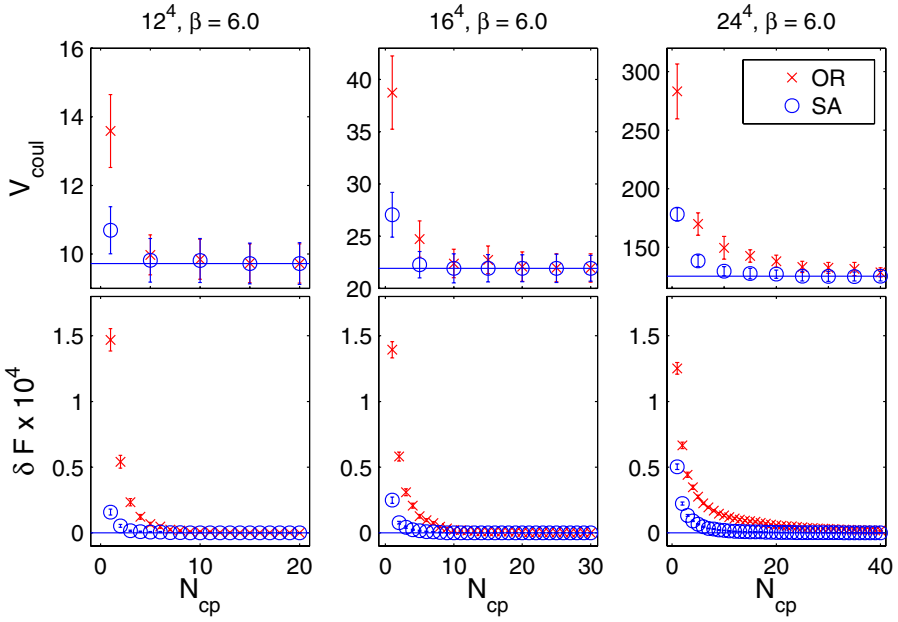

FIG. 3 (color online). The upper row shows the convergence of V_{Coul} with increasing number N_{cp} of copies obtained with either the SA-OR (circles) or the OR algorithm (crosses). The Coulomb potential is shown for the smallest (on-axis) lattice momentum available for each of the three lattice sizes, i.e. $\vec{k} = ([1, 0, 0])$ with square brackets indicating that the average over all permutations is taken. The lower row shows the corresponding convergence of the (average) deviation of the gauge functional from its best value known for each configuration. As a function of $N_{\mathrm{cp}} < N_{\mathrm{cp}}^{\mathrm{max}}$, the values of V_{Coul} and F are to be understood as those for the "currently best" gauge copy among the N_{cp} copies inspected for each configuration after N_{cp} repetitions of gauge fixing.

rithm than for the OR algorithm. With both algorithms, one needs to consider more gauge copies with growing L. For example, if we use the SA-OR algorithm, a number of copies $N_{\mathrm{cp}} = 5$ on a 12^4 lattice and $N_{\mathrm{cp}} = 15$ on a 24^4 lattice is sufficient. In contrast, if we were using the OR algorithm, $N_{\mathrm{cp}} = 40$ or more copies are necessary for a lattice like 24^4. Note that the observed increase with L at fixed β is partly due to the smaller physical value associated with the lowest on-axis lattice momentum that needs to be considered with increasing L.

On the larger lattices 32^4 and 48^4 we could not afford to gauge-fix more than a single gauge copy per configuration with the SA-OR algorithm. This was simply due to a drastic increase of the necessary number of iterations, but also due to a growing number of "trouble-making" time slices encountered on those larger lattices. Thus, we did not apply the OR algorithm for the purpose of comparison, and therefore we are not in the position to assess the influence of Gribov copies on these lattices at the present stage.

As mentioned above, we also used the fc-bc strategy to estimate the impact of Gribov-copy effects on the Coulomb potential data at different physical momenta. For this purpose we gauge fixed our field configurations at $\beta = 5.8$, 6.0, and 6.2 to Coulomb gauge only once with the OR algorithm on one hand and N_{cp} times with the SA-OR algorithm on the other. In order to obtain the results shown in Fig. 4 we have chosen, referring to Fig. 3, $N_{\mathrm{cp}} = 10$, 15, and 20 as sufficient numbers of gauge-fixed copies per configuration for the lattice sizes 12^4, 16^4, and 24^4, respectively. Then the Coulomb potential was measured separately on the set of single copies obtained with the

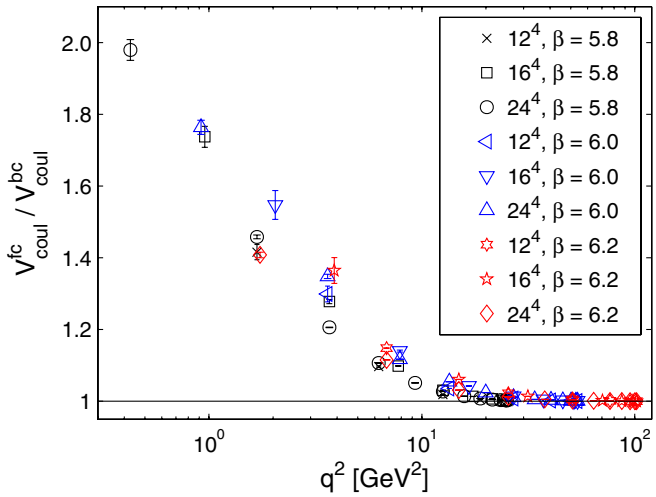

FIG. 4 (color online). The ratio of the Coulomb potential (as a function of q^2) if evaluated either on arbitrary (first) copies from simple OR or on best gauge copies from repeated SA-OR. Note that the enhancement for the first copy tremendously grows with $q^2 \to 0$ compared to what is known in the case of the ghost propagator. In contrast to the upper panel of Fig. 3, only momenta are included that are allowed by the cuts mentioned above.

OR algorithm on one hand and on the set of best copies obtained with the repeated SA-OR algorithm on the other. For brevity we refer below to these two sets as the first OR and the best SA-OR copies.

The ratio of the effective Coulomb potential measured for first OR copies and best SA-OR copies is depicted in Fig. 4 as a function of momentum squared. The Gribov ambiguity has a dramatic impact on the effective Coulomb potential at $q^2 < 10$ GeV^2. Even for the rather small lattices considered here, and hence for rather high physical momenta, the measurement of the effective Coulomb potential on first OR copies gives results larger by up to 100% than the results on best SA-OR copies. Note that this effect is much stronger than what has been observed for the ghost propagator using the same method [20,21]. There an enhancement of about 5% to 10% was typical for the presently accessible lowest momenta. Note also that here we are comparing the standard with one of the best presently known methods of gauge fixing.

In order to assess next the difference between V_{Coul} obtained from an arbitrary, first SA-OR copy (fc) and the best among a sufficient number of SA-OR copies (bc), restricted, however, to the smallest lattice momentum for each lattice size, i.e. $\vec{k} = ([1, 0, 0])$, we have to look back to Fig. 3. Considering the ratio R of the effective Coulomb potential measured either for first or best SA-OR copies as a function of the lattice size L, we find that this is well described by $R \approx c - d/L$. If such an ansatz was used to extrapolate the ratio R at $\beta = 6.0$ to $L = 48$, a ratio $R = 1.6$ would be obtained. For the first OR copy an overestimation factor $R = 2.7$ would be expected. Both are reasonable upper bounds for the overestimation of the Coulomb potential at any fixed physical momentum for first SA-OR copies and—even worse—first OR copies. This estimate will be needed in the next Sec. IV.

We conclude that the effective Coulomb potential is less affected by Gribov-copy effects if we use the SA-OR algorithm instead of the OR algorithm. This conclusion rests on the observation that the quasiconvergence of the Coulomb potential is faster for the SA-OR than for the OR algorithm. Second, the results obtained on arbitrary, first SA-OR copies (fc) are less affected by the Gribov ambiguity than those obtained on arbitrary, first OR copies. Therefore, we have used the SA-OR algorithm as our method of choice for the results to be presented in the following. Recall, however, that if only first SA-OR copies are available for analysis, measurements of the Coulomb potential in the infrared region will be accompanied with an increased uncertainty. For instance, an overestimation of about 60% for the smallest lattice momentum on a 48^4 lattice at $\beta = 6.0$ must be expected.

IV. INFRARED BEHAVIOR

Despite the Gribov ambiguity being that large, we now try to summarize what we know about the momentum dependence of the effective Coulomb potential, globally and, in particular, in the low-momentum region. As mentioned above, we were not in the position to generate more than a single SA-OR gauge copy per configuration on the larger lattices 32^4 and 48^4. Therefore we present here a full set of data concerning the Coulomb potential for a single SA-OR copy (fc) per configuration for all β values and lattices sizes, ensuring in this way an equal treatment of Gribov-copy effects on both small and large lattices. As is well known, this choice is equivalent to an averaging over all local minima of all configurations, i.e. all over the *Gribov region*. Best-copy data, that we have available only up to lattices 24^4 (after inspecting a sufficient number N_{cp} of copies) would come close to a prescription that requires an average over only the absolute minimum per configuration, i.e. restricted to the *fundamental modular region*. Zwanziger has argued that these averages should approach each other in the limit of large volumes.

As long as they did not converge, we are admitting a strong systematic effect when we restrict the analysis to the first SA-OR copy. This can be clearly seen in our data from smaller lattices, 12^4, 16^4, and 24^4. In order not to overload the Fig. 5 we show here (and lateron in Fig. 6) only *selected* results from SA-OR best copies. The data are from the 24^4 lattice where we had the choice between 40 copies at $\beta = 6.0$ and between 20 copies at $\beta = 5.8$. We try here (and later for the Coulomb potential) our best to estimate the systematic error emerging from the ignorance of further Gribov copies at larger lattices. A thorough study of the Gribov ambiguity for larger lattices remains highly desirable.

In the infrared momentum region, the running coupling given through the effective Coulomb potential diverges stronger than $1/q^2$. This is shown in the left panel of Fig. 5. The very fact of an infrared enhancement will not need to be revised if a systematic account for the Gribov effect will be undertaken in the future, although the divergence would be less pronounced. A rough indication of the size of the effect is given by the filled symbols in that figure. These are best-copy results for the lattice 24^4.

In Ref. [8], Zwanziger presented an analytic calculation of the Coulomb potential. By only considering the disconnected part of the expectation value of the effective Coulomb potential [cf. Eq. (13)] Zwanziger predicted an almost linearly rising effective Coulomb potential in the infrared limit. Using our data for the ghost propagator [20] we are now in the position to test the validity of his factorization hypothesis. If Zwanziger's assumption were valid, the ratio

$$F_{\mathrm{Coul}}(q) = \frac{V^L_{\mathrm{Coul}}(q)}{(aqG^L(q))^2} \tag{20}$$

should be constant as a function of the momenta. Note that V^L and G^L denote the bare lattice Coulomb potential and the lattice ghost propagator taken at the *physical* momen-

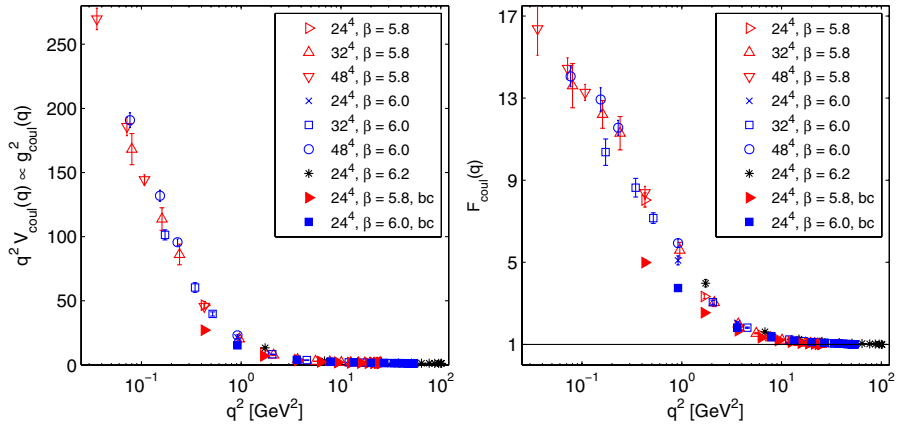

FIG. 5 (color online). Left: The running coupling $g^2_{\mathrm{Coul}}(q) \propto q^2 V_{\mathrm{Coul}}(q)$ diverges in the infrared region and tends to zero in the asymptotic limit $q^2 \to \infty$. Right: The factorization of the effective Coulomb potential is violated for momenta $0.04\ \mathrm{GeV}^2 \leq q^2 \leq 10\ \mathrm{GeV}^2$. For both the running coupling and the test of the factorization hypothesis, the open symbols (including stars) represent measurements on the first SA-OR copies per configuration. For comparison, the filled triangles and filled squares show selected results for the best SA-OR copy (bc) per configuration for two β values on the largest lattice 24^4 where the Gribov problem was fully under control.

tum q. The resulting plot shown in the right panel of Fig. 5 demonstrates that the assumption of factorization is valid only for $q^2 > 10\ \mathrm{GeV}^2$, but it is not correct in the momentum range $q^2 \leq 10\ \mathrm{GeV}^2$. This is in agreement with the results of Langfeld and Moyaerts for SU(2) pure gauge theory [16].

Much like the enhancement of the running coupling, our conclusion that the factorization hypothesis is violated would also not be invalidated if the effect of Gribov copies was taken into account properly. Similar to the left panel, the anticipated Gribov effect on the violation of factorization is shown by the filled symbols in the right panel, which are the best-copy results for the lattice 24^4.

We discuss now the momentum dependence of the effective Coulomb potential in three clearly emerging momentum ranges, the *high-momentum range*, the *intermediate momentum range*, and the *low-momentum range*, and describe the influence of the Gribov ambiguity in each range separately.

The left panel of Fig. 6 shows the presently known picture concerning the momentum dependence of $q^4 V_{\mathrm{Coul}}(q)$. A logarithmic momentum scale has been chosen in order to give a global view including the ultraviolet and infrared behavior. For the largest momenta in the *high-momentum range* $q^2 \geq 10\ \mathrm{GeV}^2$, the Coulomb potential shows roughly the expected $1/q^2$ behavior leading to an increase of $q^4 V_{\mathrm{Coul}}(q)$ linear in q^2. From Fig. 4 it is clear that the high-momentum region is robust with respect to the Gribov ambiguity. Although the inspection by eye suggests that we are seeing the tree level form of the Coulomb potential, we could not find reasonable fits of our data by the one-loop or the two-loop expressions given in Eq. (18). We conclude that much higher momenta must be considered to get an estimate of the Coulomb scale parameter Λ_{Coul} from such a fit.

With decreasing physical momenta, the first-copy data for $q^4 V_{\mathrm{Coul}}(q)$ reach an almost flat region in the *intermediate momentum range* $0.2\ \mathrm{GeV}^2 \leq q^2 \leq 6\ \mathrm{GeV}^2$, although a little bulge is visible in the left panel of Fig. 6. If the function $q^4 V_{\mathrm{Coul}}(q)$ stayed constant on the level of $\approx 20\ \mathrm{GeV}^2$ in the limit $q^2 \to 0$, this would imply a perfect linearly confining potential corresponding to an estimate of $\sigma_{\mathrm{Coul}} \approx (890\ \mathrm{MeV})^2$. This figure is more likely an upper bound.

Indeed, if for large spatial distances r we assume the simple ansatz [15]

$$V_{\mathrm{Coul}}(r) = -\sigma_{\mathrm{Coul}} r + C/r, \tag{21}$$

this suggests a momentum behavior

$$V_{\mathrm{Coul}}(q) = \frac{8\pi\sigma_{\mathrm{Coul}}}{q^4} + \frac{4\pi C}{q^2}, \tag{22}$$

with the intercept of $q^4 V_{\mathrm{Coul}}(q)$ at $q^2 = 0$ defining the Coulomb string tension σ_{Coul}.

In the *intermediate momentum range* $0.2\ \mathrm{GeV}^2 \leq q^2 \leq 6\ \mathrm{GeV}^2$, the Gribov effect sets in and becomes apparently more severe with decreasing momentum. For instance, for the smallest (on-axis) lattice momenta on lattices of sizes 12^4, 16^4, and 24^4, we have seen in Fig. 3 that the Coulomb potential $V_{\mathrm{Coul}}(q)$ is overestimated by the first SA-OR copies compared with the best SA-OR copies (among 40 copies). For the 24^4 lattice at $\beta = 6.0$ the overestimation amounts to $\approx 40\%$. This can be extrapolated to the 48^4 lattice where the effect amounts to $\approx 60\%$. This is an upper bound for the Gribov effect experienced by $V_{\mathrm{Coul}}(q)$ at *physical* momenta that are allowed by the cylinder and cone cuts.

In agreement with these estimates it can be seen in the left panel of Fig. 6 that in the *intermediate momentum*

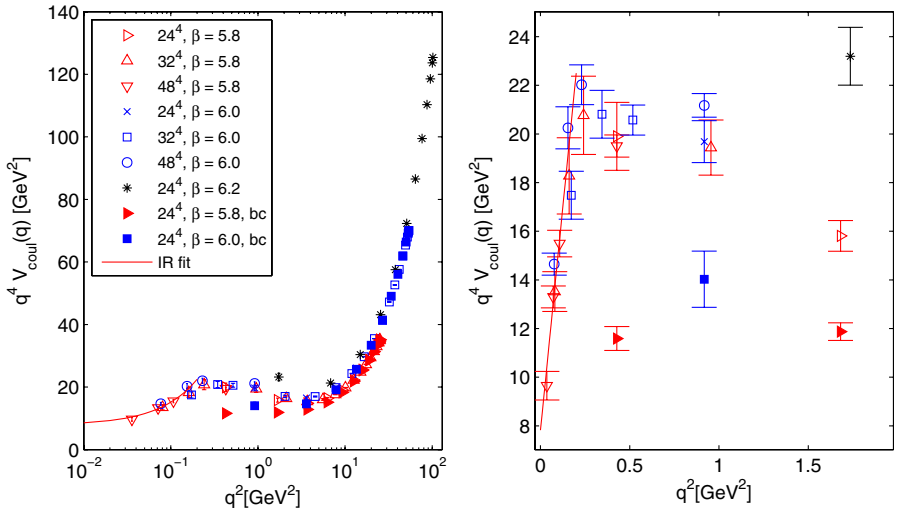

FIG. 6 (color online). The effective Coulomb potential multiplied by q^4 as a function of the physical momentum squared. Left: A logarithmic momentum scale has been chosen in order to overview both the IR and UV behavior. Right: The infrared momentum region is shown in a linear scale in q^2 in order to judge the adequacy of the linear fit of the first-copy data in the extremely IR region. The infrared fit used to extract the corresponding Coulomb string tension is also shown in the left panel. Open symbols (including stars) represent measurements on the first SA-OR copies per configuration. For comparison, the filled triangles and filled squares in both panels show results for the best SA-OR gauge copies (bc) for two β values on the lattice 24^4, the largest lattice where the Gribov problem was under scrutiny.

range 0.2 GeV$^2 \leq q^2 \leq 6$ GeV^2, the best-copy data from the 24^4 lattice (shown as filled symbols) provide us with another, independent early indication of a plateau. The somewhat lower level of ≈ 10 GeV^2 would correspond to $\sigma_{\mathrm{Coul}} \approx (630\ \mathrm{MeV})^2$. In view of this the bulge must be understood as an artifact of insufficient gauge fixing.

With the simulation reported here, on our largest lattices the *low-momentum range* with $q^2 < 0.2$ has become accessible for the first time. Rather unexpectedly in this region the first-copy data for $q^4 V_{\mathrm{Coul}}(q)$ drop with decreasing momentum as seen in the left panel. The right panel of Fig. 6 shows the infrared region magnified and in a linear scale in q^2. This picture shows that a fit ansatz linear in q^2 describes the drop of the first-copy data very well. We do not know whether a similar effect, namely, the onset of an apparently new infrared regime in the *low-momentum range* will happen for the best-copy data as well. For the time being we assume that the bulge and the new infrared regime is only a matter of measurements on insufficiently gauge-fixed configurations. We have fitted the behavior according to Eq. (22). The Coulomb string tension is estimated as

$$\sigma_{\mathrm{Coul}} = (552 \pm 35\ \mathrm{MeV})^2. \tag{23}$$

With some caution we may consider this as the *common limit* for $q^2 \to 0$ and the *common lower bound* for the Coulomb string tension (common to both standards of gauge fixing).

The other fit parameter, the "Coulombic" coefficient C in front of the $1/r$ term in Eq. (21), is obtained as

$$C = 6.0 \pm 1.0. \tag{24}$$

This parameter has no relation to the Coulombic part $1/r$ in Eq. (21). It rather describes the narrow momentum interval where the single-copy data probably converge to the best-copy results for $q^4 V_{\mathrm{Coul}}(q)$. The small number of data points is another reason why we give not much significance to the fit. Still, details of the least χ^2 fit of the first-copy data are shown in Table I. We remark that the choice of the upper momentum cutoff for the fitting range, q_{max}, has only weak influence on the fit results.

In units of the Wilson string tension the fit result is

$$\sigma_{\mathrm{Coul}} = (1.6 \pm 0.2)\sigma_{\mathrm{Wilson}}. \tag{25}$$

This is the tentative lower bound for the Coulomb string tension.

Our estimate for the Coulomb string tension is in agreement with Zwanziger's inequality. The relevance of this estimate is, however, faced with three sources of uncertainty.

(i) First, it relies only on first-copy data in a rather small number of data points, and the obtained χ^2/ndf

TABLE I. Results of χ^2 fits to the single-copy data at momenta $q^2 \leq q^2_{\mathrm{max}}$.

q^2_{max} [GeV^2]	No. data points	$\sqrt{\sigma_{\mathrm{Coul}}}$ [MeV]	C	χ^2/ndf
0.11	5	534(16)	6.6(3)	2.9
0.16	6	526(18)	6.8(4)	1.8
0.17	7	558(20)	5.8(2)	2.5
0.18	8	587(28)	4.9(2)	3.8

values are rather large (see Table I). The latter might be interpreted as a probable inadequacy of the assumed infrared ansatz Eq. (22). On the other hand, the right panel of Fig. 6 supports such a behavior.

(ii) Second, the weak but visible scaling violation of the effective Coulomb potential has the effect that our estimate of the Coulomb string tension would be higher if we considered higher inverse coupling constants β. The effective Coulomb potential in general slightly increases with increasing β.

(iii) Third, the strong Gribov effect is neglected in this estimate for the Coulomb string tension. If we had consequently looked for the best SA-OR copies and had measured $q^4 V_{\mathrm{Coul}}(q)$ for these, the amount of overestimation by the first-copy data in the bulge region is of the estimated order. One possibility is that by the drop described by the fit given above the (yet unknown) level of the best-copy results is reached. However, we cannot exclude the possibility that the best-copy data in the *low-momentum range* will also enter a new infrared regime with a similar decrease, such that the overestimation by the first-copy data remains. In this case the final estimate of the Coulomb string tension would be close to the Wilson string tension.

In the light of these uncertainties, we find it difficult to draw a conclusion on the exact value of the Coulomb string tension. Our value is larger than the values reported in previous SU(2) investigations starting also from the definition Eq. (1). These authors arrived at an estimate close to the Wilson string tension [15,16]. However, the Gribov-copy problem for the effective Coulomb potential was ignored in these studies. Furthermore, in Ref. [15] the estimate of the Coulomb string tension actually relies on data in the perturbative region, while the first plateau of $q^4 V_{\mathrm{Coul}}(q)$ has been considered as a finite-volume effect. Such a plateau could be observed in Ref. [16] but the further decrease of $q^4 V_{\mathrm{Coul}}$ for even lower momenta was beyond the possibilities of this investigation. In contrast, SU(3) studies using incomplete (partial-length) Polyakov lines, made in order to interpolate between the Coulomb string tension and the Wilson string tension, gave $\sigma_{\mathrm{Coul}} = (2\text{–}3)\sigma_{\mathrm{Wilson}}$ [10,11]. These studies also have neglected the problem of Gribov copies that might have affected the measured correlators.

V. CONCLUSIONS

In this study we have attempted a thorough measurement of the effective Coulomb potential in SU(3) lattice gauge theory. We used a broad range of lattice sizes, 12^4–48^4, to perform Monte Carlo simulations at the three values $\beta = 5.8$, 6.0, and 6.2. This has allowed us to show that finite-volume effects are hardly visible on the larger lattices and discretization effects are modest. Additionally, the use of the fc-bc strategy has revealed a dramatic dependence of the Coulomb potential on the choice of Gribov copy.

Unfortunately, by computer resources we were forced to restrict this "Gribov analysis" to the smaller lattices 12^4, 16^4, and 24^4. Thus, performing a full Gribov study up to the largest lattices still remains a highly desirable goal. We note that the necessity of choosing best copies versus first (and hence arbitrary) gauge-fixed copies is a matter of current debate (see also [25,26]). As another example, in a Becchi-Rouet-Stora-Tyutin (BRST) formulation [27], an average over all Gribov copies is taken which, on the lattice, usually leads to the well-known Neuberger $0/0$ problem [28,29]. For a recent lattice BRST formulation without this complication, see [30].

What can be said here with confidence is that for the effective Coulomb potential we find an extraordinarily strong Gribov-copy effect which has never been observed before for other observables (say, the gluon and ghost propagators).

We see a strong violation of the factorization hypothesis for the effective Coulomb potential in momentum space below $q^2 \sim 5\ \mathrm{GeV}^2$. For smaller momenta the "connected part" of the corresponding expectation value in Eq. (13) is not negligible anymore. This spoils any simple relation between the momentum dependence of the effective Coulomb potential and the behavior of the ghost propagator.

Using only one SA-OR gauge copy per configuration and hence allowing a strong systematic Gribov effect to be included in the bargain, we found a new infrared regime of the effective Coulomb potential. The first plateau of $q^4 V_{\mathrm{Coul}}(q)$, encountered with decreasing momenta, turns out *not* to represent the asymptotic behavior, because there is a further steplike decline for even smaller momenta. The size of the step is of the same order as the extrapolated difference between single-copy and many-copy SA-OR results. Therefore, we adopted the point of view that the "breakthrough" to some new infrared regime at large enough volume is a feature only of the single-copy data, and that some kind of convergence (between averaging over the Gribov region and the fundamental modular region) is behind this observation.

Future studies shall scrutinize whether the presumed common infrared limit of these two schemes really exists or, alternatively, the Gribov ambiguity persists at lower momentum for larger volumes. We estimated the Coulomb string tension by fitting the data at the lowest momenta and found it approximately 1.6 times larger than the Wilson string tension. If the Gribov ambiguity persists, it is not excluded that in the—further delayed—infrared limit finally $\sigma_{\mathrm{Coul}} = \sigma_{\mathrm{Wilson}}$ will be found.

ACKNOWLEDGMENTS

This work is supported by the DFG under Contract No. FOR 465 (Research Group *Lattice Hadron*

Phenomenology), and by the Australian Research Council. A major part of the simulations were done on the IBM pSeries 690 at HLRN, Germany. We thank H. Stüben for contributing parts of the code. We are grateful to Y. Nagakwa, A. Nakamura, T. Saito, L. von Smekal, and H. Toki for inspiring discussions.

[1] J. Greensite, Prog. Part. Nucl. Phys. **51**, 1 (2003).
[2] R. Alkofer and L. von Smekal, Phys. Rep. **353**, 281 (2001).
[3] V. N. Gribov, Nucl. Phys. **B139**, 1 (1978).
[4] D. Zwanziger, Nucl. Phys. **B518**, 237 (1998).
[5] J. Greensite, S. Olejnik, and D. Zwanziger, J. High Energy Phys. 05 (2005) 070.
[6] Y. Nakagawa, A. Nakamura, T. Saito, and H. Toki, Phys. Rev. D **75**, 014508 (2007).
[7] D. Zwanziger, Phys. Rev. Lett. **90**, 102001 (2003).
[8] D. Zwanziger, Phys. Rev. D **70**, 094034 (2004).
[9] J. Greensite and S. Olejnik, arXiv:hep-lat/0309172.
[10] Y. Nakagawa, A. Nakamura, T. Saito, H. Toki, and D. Zwanziger, Phys. Rev. D **73**, 094504 (2006).
[11] A. Nakamura and T. Saito, Prog. Theor. Phys. **115**, 189 (2006).
[12] J. Greensite, S. Olejnik, and D. Zwanziger, Nucl. Phys. B, Proc. Suppl. **141**, 199 (2005).
[13] J. Greensite, S. Olejnik, and D. Zwanziger, Phys. Rev. D **69**, 074506 (2004).
[14] J. Greensite and S. Olejnik, Phys. Rev. D **67**, 094503 (2003).
[15] A. Cucchieri and D. Zwanziger, Nucl. Phys. B, Proc. Suppl. **119**, 727 (2003).
[16] K. Langfeld and L. Moyaerts, Phys. Rev. D **70**, 074507 (2004).
[17] P. Watson and H. Reinhardt, arXiv:0711.2997.
[18] S. Necco and R. Sommer, Nucl. Phys. **B622**, 328 (2002).
[19] A. Sternbeck, E. M. Ilgenfritz, M. Müller-Preussker, and A. Schiller, Phys. Rev. D **72**, 014507 (2005).
[20] A. Voigt, E.-M. Ilgenfritz, M. Müller-Preussker, and A. Sternbeck, Proc. Sci., LAT2007 (2007) 338 [arXiv:0709.4585].
[21] E.-M. Ilgenfritz, M. Müller-Preussker, Y. Nakagawa, A. Nakamura, T. Saito, A. Sternbeck, H. Toki, and A. Voigt (unpublished).
[22] D. B. Leinweber, J. I. Skullerud, A. G. Williams, and C. Parrinello (UKQCD Collaboration), Phys. Rev. D **60**, 094507 (1999).**61**, 079901(E) (2000).
[23] A. Cucchieri and D. Zwanziger, Phys. Rev. D **65**, 014002 (2001).
[24] T. D. Bakeev, E. M. Ilgenfritz, V. K. Mitrjushkin, and M. Müller-Preussker, Phys. Rev. D **69**, 074507 (2004).
[25] I. L. Bogolubsky, G. Burgio, M. Müller-Preussker, and V. K. Mitrjushkin, Phys. Rev. D **74**, 034503 (2006).
[26] I. L. Bogolubsky *et al.*, Phys. Rev. D **77**, 014504 (2008); **77**, 039902(E) (2008).
[27] C. Becchi, A. Rouet, and R. Stora, Ann. Phys. (N.Y.) **98**, 287 (1976).
[28] H. Neuberger, Phys. Lett. B **175**, 69 (1986).
[29] H. Neuberger, Phys. Lett. B **183**, 337 (1987).
[30] L. von Smekal, D. Mehta, A. Sternbeck, and A. G. Williams, Proc. Sci., LAT2007 (2007) 382 [arXiv:0710.2410].